ADVANCED FUNCTIONAL MATERIALS
www.afm-journal.de

Improving Graphene Diffusion Barriers via Stacking Multiple Layers and Grain Size Engineering

*Susmit Singha Roy and Michael S. Arnold**

It is shown that the performance of graphene diffusion barriers can be enhanced by stacking multiple layers of graphene and increasing grain size. The focus is on large-area barriers of graphene grown by chemical vapor deposition (CVD) in the context of passivating an underlying Cu substrate from oxidation in air at 200 °C and use imaging Raman spectroscopy as a tool to temporally and spatially map the barrier performance and to guide barrier design. At 200 °C in air, Cu oxidation proceeds in multiple regimes: first slowly via transport through atomic-scale grain boundary defects inherent to CVD-graphene and then more rapidly as the graphene itself degrades and new defects are formed. In the initial regime, the graphene passivates better than previously reported. Whereas oxidation through single sheets primarily occurs through grain boundaries, oxidation through multiple sheets is spatially confined to their intersection. Performance further increases with grain-size. The degradation of the graphene itself at 200 °C ultimately limits high temperature but suggests superior low temperature barrier performance. This study is expected to improve the understanding of mass transport through CVD-graphene materials and lead to improved large area graphene materials for barrier applications.

1. Introduction

Recent experimental and theoretical work show that the one atom thick, densely packed sp^2-honeycomb network of graphene makes it nearly impenetrable to species even as small as atomic He.[1] Graphene has been found to be thermally stable even over 2600 K in inert and ultra-high vacuum environments,[2] and other experimental studies also suggest its extraordinary durability at high temperatures.[3–6] Additionally, research has shown that the atomic membrane is electrochemically inert over a wide range of potentials when used as an electrode in display devices.[7,8] Moreover, graphene can be transferred onto arbitrary substrates, is over 97% transparent, and can be scaled to areas as large as 30 inch (diagonal) via chemical vapor deposition (CVD).[9–11] These attributes inherently make graphene and graphene based materials appealing candidates for diffusion barriers in applications including the corrosion inhibition of reactive/refined metals, lifetime enhancement of organic photovoltaic devices (OPV), and ultrasensitive gas detection.[12–19]

Initial research by Compton et al. has demonstrated that nanosheets of graphene when used as a filler material in polymer films can significantly enhance its barrier properties.[20] A recent pioneering experimental study by Chen et al. has shown that large-area CVD-grown atomic membranes of graphene can be used to reduce the oxidation of refined metals even at elevated temperatures up to 200 °C.[15] Kang et al. have also shown similar results using reduced graphene oxide[16] and Yu et al.[21] have utilized 30–40 nm thick layers of self-assembled graphene oxide (GO)-polyethleneimine (PEI) composites on PET to reduce the oxygen transmission rate (OTR) to 0.05 cc/m^2-day. In addition, Kirkland et al.[22] have demonstrated that mixed-thickness CVD-graphene coatings on Ni and Cu can serve as barriers to electrochemical corrosion in aqueous media. Furthermore, Prasai et al. have shown that multiple layers of CVD-graphene can have a multiplicative effect and act as a better diffusion barrier than a single layer.[13] However, while these demonstrations of large-area graphene barriers have served as an important proof-of-principal, thus far, their performance has still been substantially below their theoretical limit.

The first practical challenge in implementing graphene as a large-area diffusion barrier is that, because it is only one atomic layer, even a single defect has the possibility of providing a spurious transport pathway for leakage across its thickness. CVD-graphene, while attractive for its scalability, is known in particular to be punctuated by microscopic (tears and holes) and atomic-scale (grain boundary) defects. In principal, it should be possible to eliminate tears and holes by refining the purity and smoothness of the Cu growth substrates, processing in more particulate-free environments, and developing better graphene transfer procedures. On the other hand, grain boundaries will always be ubiquitous in polycrystalline CVD-graphene. It has been theoretically shown by Topsakal et al. that grain boundary defects can act as spurious diffusion pathways for oxygen transport.[14] Chen et al.[15] have imaged the oxidation of Cu through single layers of graphene and shown that the Cu oxidizes in a pattern that appears to be related to the grain boundaries of the graphene, but the correlation between grain boundaries and oxidation was not explicitly confirmed.

S. Singha Roy, Prof. M. S. Arnold
Department of Materials Science and Engineering
University of Wisconsin–Madison
1509 University Avenue
Madison, WI 53706, USA
E-mail: msarnold@wisc.edu

DOI: 10.1002/adfm.201203179

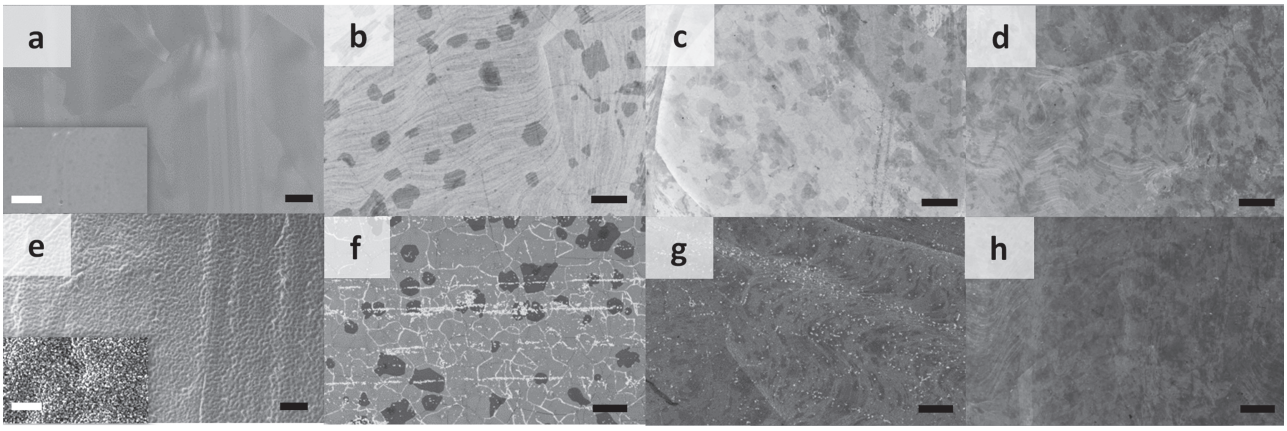

Figure 1. SEM images comparing bare Cu, SLG*x*1_Cu, SLG*x*2_Cu, and SLG*x*4_Cu before (a–d, respectively) and after (e–h, respectively) 240 min of annealing in air at 200 °C. Scale bars = 10 μm. Insets in (a) and (e) depict SEM images of wider areas. Scale bars = 1 μm.

A second practical challenge is stability. While graphene has excellent stability in inert environments,[2] it is less stable under oxidizing conditions. Preliminary studies have shown that the interior of a grain of CVD-graphene will degrade rapidly at 400 °C in air.[23,24] Degradation in ambient at temperatures <400 °C may be possible but has not been elucidated in detail. Grain boundaries and defects are expected to further decrease stability. Xu et al. have shown via modeling that the oxidative etching of graphene at a defect site is expected to be faster than at a non-defect site.[25] Duong et al. have experimentally shown that grain boundaries in CVD-graphene on Cu can be probed when it is exposed to UV radiation in ambient because UV-generated O and OH radicals will selectively react with and degrade the graphene grain boundaries thereby providing an enhanced pathway for the oxidization of the underlying Cu substrate.[26] In general, if there is instability and degradation of graphene or its grain boundaries under a particular set of conditions then this will further limit the applicability of graphene as a diffusion barrier under these conditions.

Here, in order to gain more insight into these aspects, we have used imaging Raman spectroscopy to conduct detailed measurements of the oxidation of Cu through single and multiple layers of graphene, grown via CVD. We have used imaging Raman spectroscopy, in particular, as a tool to map where the oxidation occurs and to also track how both the oxidation and stability of the graphene evolve with time.

2. Results and Discussion

The graphene barriers for our studies were grown one layer at a time on Cu foils using standard atmospheric pressure CVD commonly used to grow monolayer graphene.[27,28] Here, we refer to single layered graphene (SLG) on Cu by the abbreviation, SLG*x*1_Cu. Two-layered (SLG*x*2_Cu) and four-layered (SLG*x*4_Cu) samples were fabricated by mechanically transferring additional layers of graphene onto the SLG*x*1_Cu with the help of a sacrificial layer of poly(methyl methacrylate), using a transfer approach derived from that of Li et al., Safron et al., and others for transferring graphene to arbitrary substrates.[12,29,30] All multi-layered samples were fabricated using graphene with 3 μm grains. The motivation behind independently growing then post-synthetically stacking the layers was to ensure a misalignment of microscopic and atomic-scale defects in each layer. The graphene on Cu samples (collective term for SLG*x*1_Cu, SLG*x*2_Cu and SLG*x*4_Cu) and control Cu samples without graphene were heated on a hotplate set to 200 °C in ambient atmosphere for up to 10 h, in order to induce oxidation. A temperature of 200 °C was used to ensure rapid Cu oxidation kinetics and to match the work of Chen et al.[15] After oxidation, the samples were imaged using scanning electron microscopy (SEM) and the oxidation of the Cu was quantified temporally and spatially using imaging Raman spectroscopy. Cu_2O was specifically mapped via its well established Raman mode at ≈647 cm^{-1} and grain boundaries and defects in graphene were mapped by the D-band Raman mode at ≈1345 cm^{-1}.[31–35] To quantify oxidation for the kinetics studies, the Cu_2O Raman intensity was averaged spatially over a 20 × 20 μm^2 region for the 3 μm grain size and a 30 × 30 μm^2 region for 14 μm sized grains. In order to independently confirm the Raman data, X-ray photoelectron spectroscopy (XPS) and X-ray excited Auger electron spectroscopy (XAES) were performed on a subset of samples, although the approaches only provide macroscopic averages of the degree of Cu oxidation (see Figures S1–3 and Table 1 in the Supporting Information).

Figure 1a–d show electron microscopy images of annealed Cu foil without graphene and SLG*x*1_Cu, SLG*x*2_Cu and SLG*x*4_Cu substrates, respectively, prior to oxidation. The bare annealed Cu foil was polycrystalline and relatively smooth, and the morphology of the graphene modified Cu substrates was similar. The regions of darker contrast in the images of the graphene modified Cu show the partial growth of additional layers. For example, the regions of darker contrast in the SLG*x*1 image (Figure 1b) correspond to partial second layers.

Figure 1e–h show electron microscopy images of annealed Cu foil without graphene and SLG*x*1_Cu, SLG*x*2_Cu and SLG*x*4_Cu substrates, respectively, after 240 min of annealing in air. The surface of the Cu foil without graphene nearly completely oxidizes and becomes considerably rougher. In contrast, there is significantly less oxidation or perturbation

of the graphene on Cu samples. Two features are observed in the SLG*x*1_Cu samples: i) an interconnected network or grain boundary-like web of oxidation and ii) oxidation along horizontal striations. The former resembles the observations of Chen et al.,[15] which we later confirm correspond to oxidation of the underlying Cu directly through graphene's grain boundaries, via Raman mapping. The latter occurs at macroscopic striations in the Cu foil that result from the foil's processing and manufacture that translate into defects/steps into the structure of the graphene. In principal, these striations could be eliminated prior to CVD.

In comparison to the SLG*x*1_Cu samples, there is considerably less oxidation of the SLG*x*2_Cu samples and SLG*x*4_Cu samples (Figure 1g,h) where the oxidation furthermore occurs in a different way. The Cu oxidation is limited to single points in SLG*x*2_Cu samples whereas considerable oxidation is not observed at all in SLG*x*4_Cu samples. Qualitatively, the improved barrier performance of the multilayers makes sense as the microscopic and atomic-scale defects in each layer will be incommensurate, which is discussed further later.

The degree of oxidation of each of these four samples is more quantitatively compared in **Figure 2**a, using Raman spectra to assess copper oxide yield spatially averaged over a $20 \times 20\ \mu m^2$ region. The spectrum of the highly oxidized bare foil is dominated by an intense feature at 647 cm^{-1} corresponding to Cu_2O and smaller peaks at 500 cm^{-1} and 800 cm^{-1} for CuO and $Cu(OH)_2$ respectively. In comparison, the Cu_2O Raman feature is 41, 73, and >403 times weaker on the SLG*x*1_Cu, SLG*x*2_Cu, and SLG*x*4_Cu, respectively. In the SLG*x*4_Cu sample, the graphene G- and 2D-band Raman features are visible at ≈1585 cm^{-1} and ≈2670 cm^{-1}, respectively, but the Cu_2O Raman feature is immeasurable, below the noise. It should be noted that that the 2D/G ratio of the SLG*x*2_Cu and SLG*x*4_Cu spectra are decreased with respect to that of the SLGx1_Cu sample. This change is observed both before and after annealing at 200 °C and can be attributed inter-layer interactions between domains of graphene that are randomly oriented.[36–38]

To better understand how the oxidation yield of each of these samples evolves, we measured similar Raman spectra as a function of time at intervals up to 610 min of oxidation (Figure 2b). The kinetics plots show that the amplitude of the Cu_2O Raman feature increases rapidly on the bare Cu sample, saturating after only ≈5 min (Figure 2b). In contrast, the amplitude of the Cu_2O Raman feature increases much more slowly on the graphene on Cu samples, although the increase is not linear. For example, at first, the increase in amplitude of the Cu_2O Raman feature on the SLG*x*1_Cu substrate is 290× slower than the bare Cu substrate. But, after ≈60 min, the oxidation accelerates. Then, after ≈240 min, the oxidation tends to saturate but at only ≈10% of the amplitude of the bare Cu substrates. The mechanisms responsible for these three regimes of oxidation are discussed further later.

The kinetics plots for the SLG*x*2_Cu and SLG*x*4_Cu samples show that the rate of Cu oxidation is increasingly suppressed with an increasing number of sheets. In particular, at any given time, the overall degree of oxidation of the SLG*x*2_Cu and SLG*x*4_Cu samples is less than that of SLG*x*1_Cu samples. Furthermore, the onset of the accelerated degradation is delayed. For example, the first clearly measurable signature of oxidation

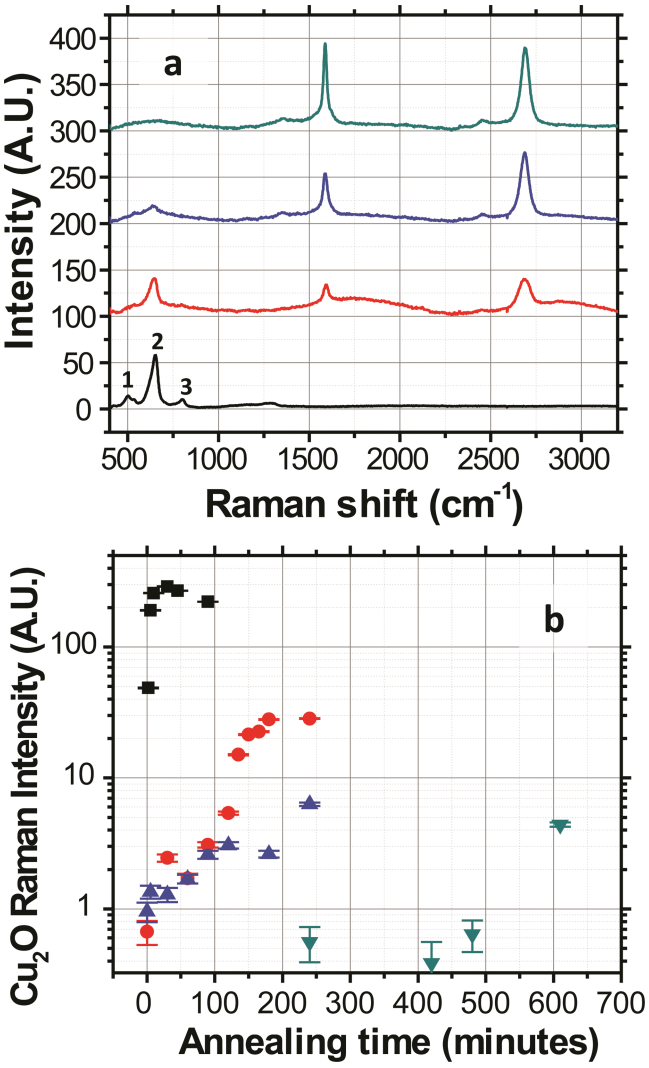

Figure 2. a) Raman spectra of bare Cu, SLG*x*1_Cu, SLG*x*2_Cu, and SLG*x*4_Cu after 240 min in air at 200 °C, offset from bottom to top, respectively. Legend for bare Cu spectra: 1–500 cm^{-1} (CuO), 2–647 cm^{-1} (Cu_2O), 3–800 cm^{-1} ($Cu(OH)_2$. b) Kinetic evolution of the Cu_2O Raman feature at 647 cm^{-1} for bare Cu (black squares), SLGx1_Cu (red circles), SLGx2_Cu (blue triangles), and SLGx4_Cu (inverted green triangles). Error bars depict ± one standard deviation in fitting certainty of the amplitude of the Cu_2O Raman feature.

of the SLG*x*4_Cu samples is not observed until 610 min. In all of the graphene on Cu samples, however, while the initial rate of oxidation was slow, it accelerated with time. Figure 2a compares the Raman spectra after 240 min of oxidation for the bare copper and the graphene on Cu samples. It can be easily noted from these spectra that the intensity of the Cu_2O peak (647 cm^{-1}) is reduced as the number of graphene layers on Cu is increased. The broad background/interference patterns between 400–1000 cm^{-1}, 1200–1900 cm^{-1} and 2500–3100 cm^{-1} are from the substrate (Cu).

In order to better understand the pathways for oxidation through single and multiple sheets of graphene, we collected Raman maps and electron micrographs of the samples at fixed

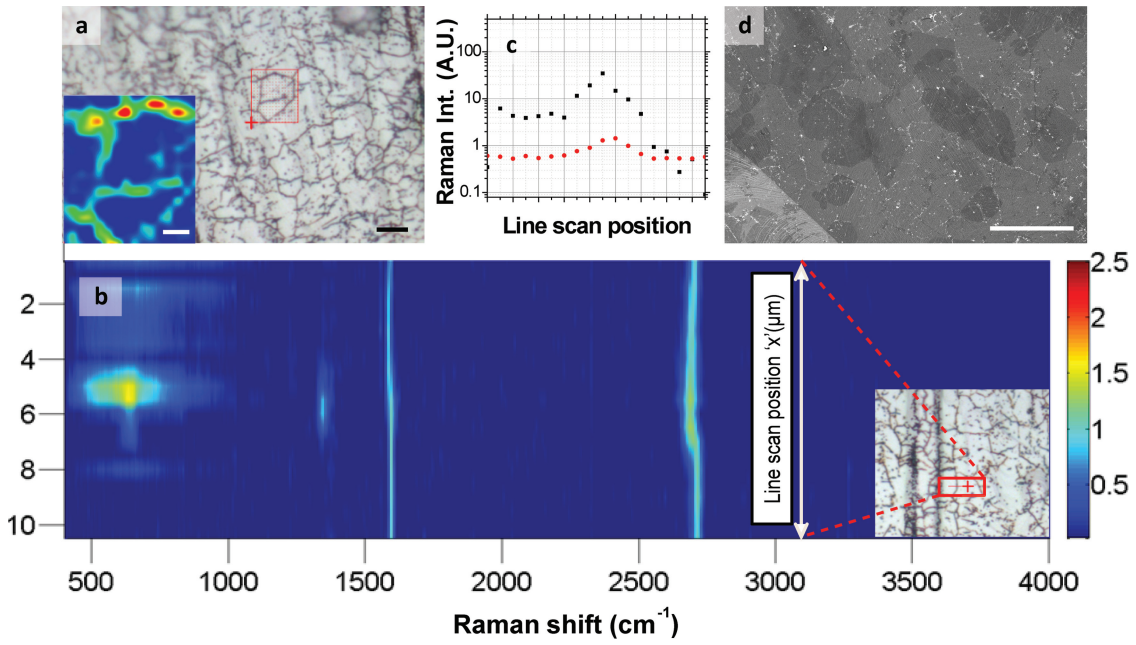

Figure 3. a) Optical microscopy image highlighting the Cu oxide features on SLGx1_Cu after 120 min (scale bar = 10 μm). Inset maps the Cu_2O Raman intensity in the region of part (a) highlighted red (scale bar = 3 μm). b) Raman line-scan across a Cu oxide feature (inset–red line), normalized to the intensity of the G-band at each point along the line-scan. c) Cu_2O peak intensity (black squares, right axis) and integrated D/G ratio (left axis) as a function of position, extracted from the Raman line-scan in part b). The Cu_2O peak intensity was extracted from the Raman scattering signal at 647 cm^{-1} from the line-scan from part (b) and the integrated D/G ratio was extracted by integrating the Raman signal due to the D-peak at 1345 cm^{-1} and dividing by the integrated Raman signal due to the G-peak at 1585 cm^{-1} from the line-scan from part (b). d) SEM of oxidized SLGx2_Cu sample. The faint white lines are Cu oxide resulting from lateral diffusion between the two graphene layers and the subsequent oxidation of the Cu at the grain-boundaries of the graphene layer immediately in contact with the Cu (scale bar = 10 μm).

oxidation times. We first analyzed a SLG*x*1_Cu sample prior to oxidation (see Figure S4,5 in the Supporting Information). We then analyzed a SLG*x*1_Cu after 120 min of oxidation. A map of the Cu_2O Raman feature intensity at 647 cm^{-1} and a corresponding optical micrograph of the same region confirm that the web of topographical features observed optically and in the SEM are indeed Cu_2O (**Figure 3**a and inset). The Raman mapping offers the possibility for not only mapping the spatial distribution of Cu_2O but for also mapping the spatial distribution of defects in the graphene via its D-band, at the same time. Toward this end, we measured high resolution Raman spectra at a number of points along a line intersecting one of the oxide features (Figure 3b, inset). The resulting two-dimensional Raman map (with color intensity normalized to the graphene G-band) is shown in Figure 3b, whereas Figure 3c presents the intensity of the Cu_2O (647 cm^{-1}) and the D-band spectral features (normalized to the G peak) as function of position. The data show that the Cu_2O is commensurate with a concentration of defects in the graphene. This data taken together with knowledge of the characteristic grain-size of the graphene (3 μm) conclusively confirms that oxidation through single layers of graphene occurs primarily through its grain boundaries, thereby resulting in oxide directly underneath them.

It then follows that in multilayered samples, these "line-of-sight" pathways would be reduced primarily to a set of points where the defect/grain boundaries of all the stacked layers coincide. For example, oxidation through two layers would be reduced to a set of points only where the grain boundaries of the two stacked layers intersect. Oxidation through multiple layers also has the possibility of proceeding via a second mechanism, which is via lateral-diffusion pathways, where oxygen penetrates through the defect/grain boundary of the topmost layer and laterally diffuses between two graphene layers until it finds a defect/grain boundary in the second layer and so on until it reaches the surface of the Cu. Oxidation via the former can be easily observed in Figure 1g, whereas oxidation via the latter can be seen as faint white dotted lines (Figure 3d) indicating Cu oxidation at the grain boundaries of the layer in contact with the Cu (as seen through the overlying layer).

If the primary mode of oxygen transport through graphene is via its grain-boundaries, then it should be possible to engineer improved graphene barriers by controlling grain-size, which we demonstrate in **Figure 4**. We varied the grain-size of graphene by adjusting the growth temperature and the carbon concentration during the CVD process. The average grain-sizes were calculated by measuring the spatially averaged internucleation distance from partial growths under the same conditions. For this particular aspect of our study, we used SLG*x*1_Cu with grain sizes (or internucleation distances) of 3 μm and 14 μm (Figure 4a,b, respectively). After annealing for 240 min, one can observe the formation Cu_2O on both of the SLG*x*1_Cu's at their respective grain boundaries (Figure 4c,d, respectively). The average grain-size observed by the formation of the Cu_2O compares very well with our measurements of inter-nucleation

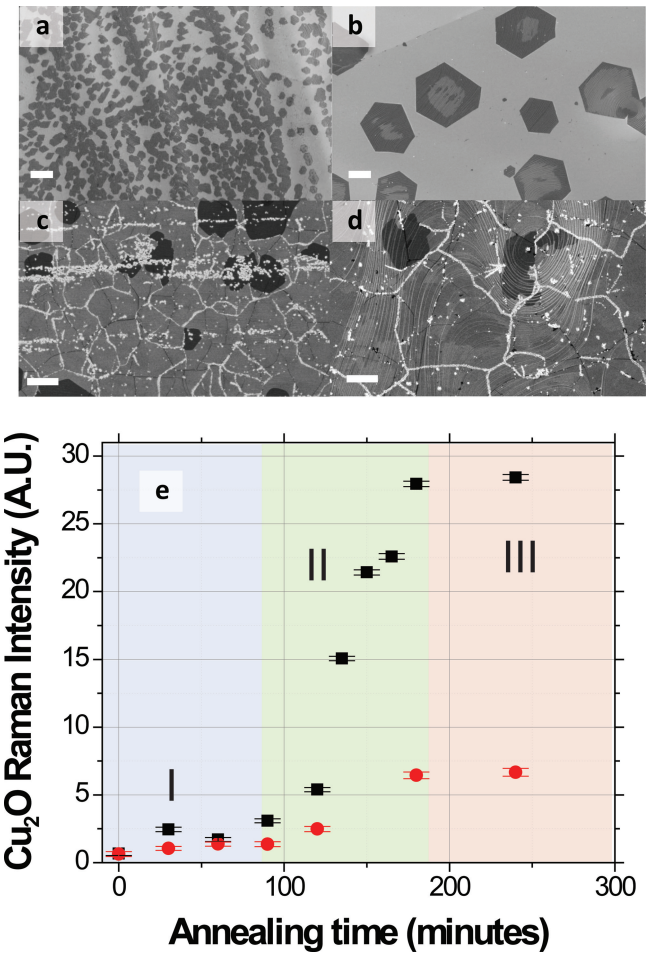

Figure 4. a,b) SEM images showing the nucleation density for partially grown graphene monolayers at 972 °C and 1030 °C, respectively (scale bars = 5 μm). c,d): SEM images of fully grown graphene layers at 972 °C and 1030 °C after 240 min of annealing on Cu at 200 °C in air. The underlying Cu locally oxidizes underneath grain boundaries in the overlying graphene indicated by the white features in the image. e) Grain size or defect density dependence of transport through a single layer of graphene: black squares and red circles represent the oxidation kinetics of SLG*x*1_Cu with 3 μm grains and SLG*x*1_Cu with 14 μm grains, respectively. Error bars depict ± one standard deviation in fitting certainty of the amplitude of the Cu_2O Raman feature.

distance. Figure 4e depicts the oxidation kinetics as a function of grain-size. The onset of oxidation occurs at roughly 90 min in both samples, but the oxidation saturates at roughly 20% of the intensity in the SLGx1_Cu sample with 14 μm grains compared with the sample with 3 μm grains. It can be inferred from the plot that the rate and degree of oxidation through a single layer of graphene are both linearly related to its defect/grain boundary density.

The kinetics plots in Figure 2 and 4e all generally tell a similar story, in which the oxidation evolves over time in three regimes, which are labeled in Figure 4e. At short times (regime I), the rate of oxidation is slowest. At moderate times (regime II), the rate of oxidation rapidly increases. Finally, at long times (regime III), the Cu_2O peak intensity tends to saturate. The latter saturation can be attributed to a self-passivation of the Cu under the graphene grain boundaries by already-formed Cu_2O, after it becomes sufficiently thick. What is not immediately clear, however, is the mechanism for the acceleration of oxidation in regime II. Our hypothesis is that the graphene itself degrades at 200 °C, thereby introducing new defects that accumulate with time, providing additional transport pathways through each sheet of graphene and accelerating oxidation.

Previous experimental studies have shown that the defect density and doping of CVD grown graphene increase with temperature and annealing time rapidly over 400 °C.[23,24,39] To study the stability of the polycrystalline CVD-graphene at only 200 °C, by itself off of the Cu substrate, we transferred a single layer of graphene onto a SiO_2/Si substrate and annealed it for 240 min in air. The defect density was monitored using Raman Spectroscopy as a function of time. The integrated D/G Raman ratio, spatially averaged over a 30 × 30 μm^2 region, was initially 0.05, which is typical of CVD-graphene (**Figure 5**a). After annealing

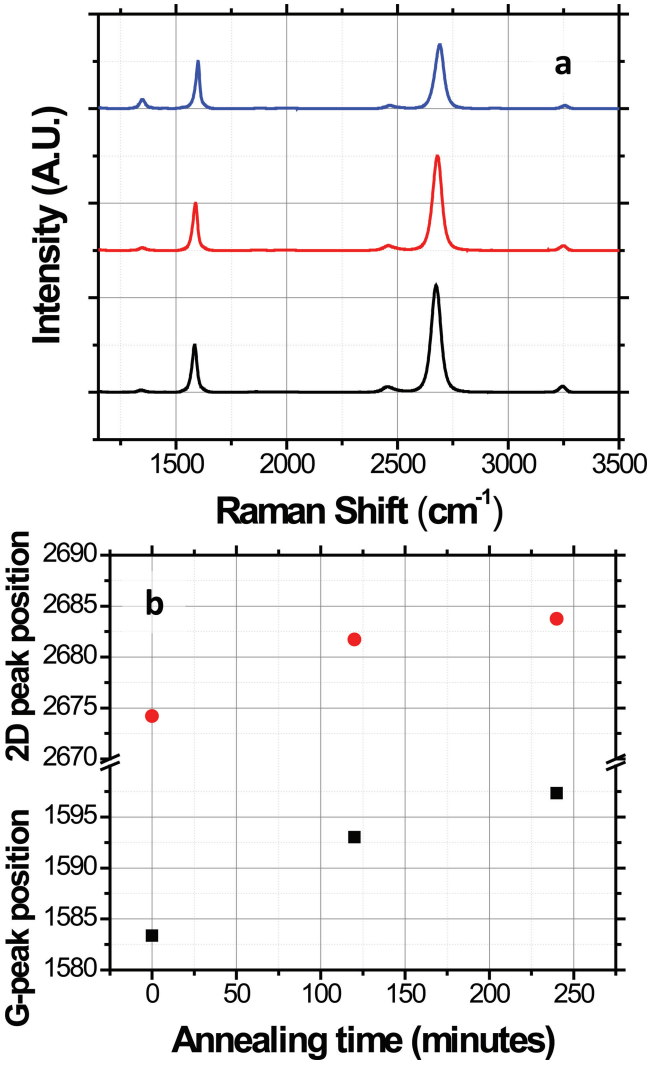

Figure 5. a) Raman spectra of CVD-graphene (normalized to G-band) on SiO_2/Si after 0 min (bottom), 120 min (middle) and 240 min (top) of annealing in air at 200 °C. b) Spectral shift of the G and the 2D Raman modes with annealing time, indicating an increase in doping with time.

for 120 min, the integrated D/G Raman ratio increased marginally to 0.06. However, after 240 min, the ratio increased to 0.19, indicating the formation of new defects. The positions of the G and 2D peaks also up-shifted with time during annealing (Figure 5b). Previous work[40] has shown that this up-shift can be attributed to a change in doping arising from oxygen and moisture exposure or coupling of the graphene layer to the substrate. Determining the exact mechanism for the decomposition of CVD-graphene with increasing temperature will be the focus of a future study. Nonetheless, this decomposition accounts for the accelerated Cu oxidation in regime II and indicates that the performance of polycrystalline graphene as a diffusion barrier at 200 °C is limited by its instability.

Thus, overall, we believe that in regime I, the oxidation primarily occurs via the defects and grain boundaries that existed in the (as-grown) graphene prior to the 200 °C annealing, or in other words, via the defects inherent to CVD-graphene. With time, these defects and grain boundaries themselves degrade and new defects are formed, further enhancing mass transport through the graphene layers–which result in a rapid increase in the Cu_2O peak intensity with annealing time in regime II. Eventually, in regime III, the Cu oxidation becomes limited not by transport through the graphene barrier layers but rather by slow transport through the existing Cu_2O, itself. Perhaps the most interesting aspect is regime I because it suggests that if the stability of the CVD-graphene can be maintained (for example, possibly at lower temperature) then substantially superior barrier performance may be achievable. In fact, in this case, the ultimate barrier performance may be even better than what we observe in regime I, here, because it is likely that in reality there is not a sharp transition between regime I and II but rather a continuous build-up of defects with time, starting as soon as at $t = 0$. More detailed studies of the stability of polycrystalline CVD-graphene and the mechanisms for its degradation as a function of temperature are needed to confirm these hypotheses.

3. Conclusion

We have utilized imaging Raman spectroscopy in conjunction with electron microscopy to better understand how the oxidation of Cu passivated by single and multiple layers of graphene, grown by chemical vapor deposition (CVD), evolves temporally and spatially. At 200 °C in air, Cu oxidation proceeds in 3 regimes: first slowly via transport through atomic-scale grain boundary defects inherent to CVD-graphene; secondly more rapidly as the graphene itself degrades and new defects are formed; and finally the oxidation saturates after the Cu_2O reaches a sufficient thickness to limit transport. The degradation limits high temperature barrier applications; however, initially, the graphene passivates substantially better than previously reported, suggesting better low temperature performance. The Raman maps establish that oxidation through single sheets occurs through graphene's grain boundaries, whereas oxidation through multiple sheets occurs via first at their intersection and then more slowly via lateral-diffusion between layers. Performance further increases with grain-size; for example, increasing grains from 3 μm to 14 μm decreases the oxidation rate by an additional factor of ≈5 per sheet, suggesting additional gains in performance will be possible with improved graphene crystal growth. Overall, this study is expected to improve the understanding of transport through CVD-graphene and lead to improved large area graphene materials for barrier applications.

4. Experimental Section

Preparation: The graphene barriers for our studies were grown one layer at a time on Cu foils using standard atmospheric pressure chemical vapor deposition (CVD) commonly used to grow monolayer graphene.[27,28] Prior to CVD, the Cu foils (Alfa Aesar 99.8% Lot # 13382) were annealed in a reducing forming gas environment (17 sccm H_2, 320 sccm Ar) at their respective growth temperatures for 30 min. The growth of graphene with 3 μm grains was achieved by adding a 0.360 sccm CH_4 flow for 240 min at 972 °C. The growth of graphene with 14 μm grains was initiated by adding a 0.250 sccm CH_4 flow for 240 min at 1030 °C. Control bare Cu samples without graphene were produced by annealing in forming gas at 972 °C for 270 min but never introducing methane. Two-layered (SLG*x*2_Cu) and four-layered (SLG*x*4_Cu) samples were fabricated by mechanically transferring additional layers of graphene onto the SLG*x*1_Cu with the help of a sacrificial layer of poly(methyl methacrylate), using a transfer approach derived from that of Li et al., Safron et al., and others for transferring graphene to arbitrary substrates.[29,30] Oxidation was carried out on a hot-plate set to 200 °C in air. The ambient temperature = 23.5 °C and the relative humidity was 32–37%.

Characterization: After oxidation, the samples were imaged using SEM (LEO 1530, 3 keV) and optical microscopy. The oxidation of the Cu was quantified temporally and spatially using imaging Raman spectroscopy (DXR Raman Microscope Thermo Scientific, excitation λ = 532 nm, 1 mW). The step size of the scans was 1 μm and the laser spot size was also ≈1 μm. The laser power and exposure time were sufficiently low so that the Raman laser did not induce oxidation of the Cu during measurement. The amplitude of the Cu_2O component of each Raman spectrum was determined by fitting. Each spectrum was fit from 450–850 cm^{-1} using the Raman spectrum of the oxidized bare Cu sample as a reference spectrum for Cu_2O and a sixth order polynomial to account for the broad background and interference effects. The full-width at half-maximum of the main Cu_2O peak at 647 cm^{-1} was only 50 cm^{-1} and could not be reproduced by the polynomial background, which was forced to fit over the entire 450–850 cm^{-1} range. Thus, this fitting protocol successfully was able to extract the Cu_2O component of each spectrum. XPS and XAES studies were performed using Perkin Elmer 5400 XPS (ESCA- electron spectroscopy for chemical analysis) with an Mg X-ray source (15 kV, 300 W).

Supporting Information

Supporting Information is available from the Wiley Online Library or from the author.

Acknowledgements

This work was supported by National Science Foundation (Grant# CBET-1033346). M.S.A. also acknowledges partial support from a 3M Non-Tenured Faculty Grant.

Received: October 30, 2012
Revised: December 21, 2012
Published online: February 26, 2013

[1] J. S. Bunch, S. S. Verbridge, J. S. Alden, A. M. van der Zande, J. M. Parpia, H. G. Craighead, P. L. McEuen, *Nano Lett.* **2008**, *8*, 2458.
[2] K. Kim, W. Regan, B. Geng, B. Aleman, B. M. Kessler, F. Wang, M. F. Crommie, A. Zettl, *Phys. Status Solidi-R* **2010**, *4*, 302.
[3] W. A. de Heer, C. Berger, X. S. Wu, P. N. First, E. H. Conrad, X. B. Li, T. B. Li, M. Sprinkle, J. Hass, M. L. Sadowski, M. Potemski, G. Martinez, *Solid State Commun.* **2007**, *143*, 92.
[4] C. Berger, Z. M. Song, T. B. Li, X. B. Li, A. Y. Ogbazghi, R. Feng, Z. T. Dai, A. N. Marchenkov, E. H. Conrad, P. N. First, W. A. de Heer, *J. Phys. Chem. B* **2004**, *108*, 19912.
[5] X. Wang, L. J. Zhi, K. Mullen, *Nano Lett.* **2008**, *8*, 323.
[6] S. Shivaraman, M. V. S. Chandrashekhar, J. J. Boeckl, M. G. Spencer, *J. Electron. Mater.* **2009**, *38*, 725.
[7] P. Blake, P. D. Brimicombe, R. R. Nair, T. J. Booth, D. Jiang, F. Schedin, L. A. Ponomarenko, S. V. Morozov, H. F. Gleeson, E. W. Hill, A. K. Geim, K. S. Novoselov, *Nano Lett.* **2008**, *8*, 1704.
[8] P. Matyba, H. Yamaguchi, M. Chhowalla, N. D. Robinson, L. Edman, *ACS Nano* **2011**, *5*, 574.
[9] S. Bae, H. Kim, Y. Lee, X. F. Xu, J. S. Park, Y. Zheng, J. Balakrishnan, T. Lei, H. R. Kim, Y. I. Song, Y. J. Kim, K. S. Kim, B. Ozyilmaz, J. H. Ahn, B. H. Hong, S. Iijima, *Nat. Nanotechnol.* **2010**, *5*, 574.
[10] A. Reina, X. T. Jia, J. Ho, D. Nezich, H. B. Son, V. Bulovic, M. S. Dresselhaus, J. Kong, *Nano Lett.* **2009**, *9*, 30.
[11] J. W. Suk, A. Kitt, C. W. Magnuson, Y. Hao, S. Ahmed, J. An, A. K. Swan, B. B. Goldberg, R. S. Ruoff, *ACS Nano* **2011**, *5*, 6916.
[12] L. G. De Arco, Y. Zhang, C. W. Schlenker, K. Ryu, M. E. Thompson, C. Zhou, *ACS Nano* **2010**, *4*, 2865.
[13] D. Prasai, J. C. Tuberquia, R. R. Harl, G. K. Jennings, K. I. Bolotin, *ACS Nano* **2012**, *6*, 1102.
[14] M. Topsakal, H. Sahin, S. Ciraci, *Phys. Rev. B* **2012**, *85*, 155445.
[15] S. Chen, L. Brown, M. Levendorf, W. Cai, S.-Y. Ju, J. Edgeworth, X. Li, C. W. Magnuson, A. Velamakanni, R. D. Piner, J. Kang, J. Park, R. S. Ruoff, *ACS Nano* **2011**, *5*, 1321.
[16] D. Kang, J. Y. Kwon, H. Cho, J.-H. Sim, H. S. Hwang, C. S. Kim, Y. J. Kim, R. S. Ruoff, H. S. Shin, *ACS Nano* **2012**, *6*, 7763.
[17] S. Singha Roy, D. J. Bindl, M. S. Arnold, *J. Phys. Chem. Lett.* **2012**, *3*, 873.
[18] P. Lange, M. Dorn, N. Severin, D. A. Vanden Bout, J. P. Rabe, *J. Phys. Chem. C* **2011**, *115*, 23057.
[19] I. P. Murray, S. J. Lou, L. J. Cote, S. Loser, C. J. Kadleck, T. Xu, J. M. Szarko, B. S. Rolczynski, J. E. Johns, J. X. Huang, L. P. Yu, L. X. Chen, T. J. Marks, M. C. Hersam, *J. Phys. Chem. Lett.* **2011**, *2*, 3006.
[20] O. C. Compton, S. Kim, C. Pierre, J. M. Torkelson, S. T. Nguyen, *Adv. Mater.* **2010**, *22*, 4759.
[21] L. Yu, Y.-S. Lim, J. H. Han, K. Kim, J. Y. Kim, S.-Y. Choi, K. Shin, *Synth. Met.* **2012**, *162*, 710.
[22] N. T. Kirkland, T. Schiller, N. Medhekar, N. Birbilis, *Corros. Sci.* **2012**, *56*, 1.
[23] B.-J. Lee, G.-H. Jeong, *J. Nanosci. Nanotechnol.* **2011**, *11*, 6084.
[24] S. P. Surwade, Z. Li, H. Liu, *J. Phys. Chem. C* **2012**, *116*, 20600.
[25] S. C. Xu, S. Irle, D. G. Musaev, M. C. Lin, *J. Phys. Chem. C* **2007**, *111*, 1355.
[26] D. L. H. Duong, G. H. Lee, S. M. Gunes, F. Kim, E. S. Kim, S. T. Kim, H. Ta, Q. S. So, K. P. Yoon, S. J. Chae, S. J. Jo, Y. W. Park, M. H. Chae, S. H. Lim, S. C. Choi, J. Y. Lee, Y. Hee, *Nature* **2012**, *490*, 235.
[27] X. S. Li, W. W. Cai, J. H. An, S. Kim, J. Nah, D. X. Yang, R. Piner, A. Velamakanni, I. Jung, E. Tutuc, S. K. Banerjee, L. Colombo, R. S. Ruoff, *Science* **2009**, *324*, 1312.
[28] J. D. Wood, S. W. Schmucker, A. S. Lyons, E. Pop, J. W. Lyding, *Nano Lett.* **2011**, *11*, 4547.
[29] X. Li, Y. Zhu, W. Cai, M. Borysiak, B. Han, D. Chen, R. D. Piner, L. Colombo, R. S. Ruoff, *Nano Lett.* **2009**, *9*, 4359.
[30] N. S. Safron, M. Kim, P. Gopalan, M. S. Arnold, *Adv. Mater.* **2012**, *24*, 1041.
[31] G. Niaura, *Electrochim. Acta* **2000**, *45*, 3507.
[32] A. C. Ferrari, *Solid State Commun.* **2007**, *143*, 47.
[33] L. M. Malard, M. A. Pimenta, G. Dresselhaus, M. S. Dresselhaus, *Phys. Rep.* **2009**, *473*, 51.
[34] D. Graf, F. Molitor, K. Ensslin, C. Stampfer, A. Jungen, C. Hierold, L. Wirtz, *Nano Lett.* **2007**, *7*, 238.
[35] S. T. Mayer, R. H. Muller, *J. Electrochem. Soc.* **1992**, *139*, 426.
[36] K. Kim, S. Coh, L. Z. Tan, W. Regan, J. M. Yuk, E. Chatterjee, M. F. Crommie, M. L. Cohen, S. G. Louie, A. Zettl, *Phys. Rev. Lett.* **2012**, *108*, 246103.
[37] R. W. Havener, H. Zhuang, L. Brown, R. G. Hennig, J. Park, *Nano Lett.* **2012**, *12*, 3162.
[38] J. Robinson, S. Schmucker, B. Diaconescu, J. Long, J. Culbertson, T. Ohta, A. Friedman, T. Beechem, *ACS Nano* **2013**, *7*, 637.
[39] L. Liu, S. Ryu, M. R. Tomasik, E. Stolyarova, N. Jung, M. S. Hybertsen, M. L. Steigerwald, L. E. Brus, G. W. Flynn, *Nano Lett.* **2008**, *8*, 1965.
[40] S. Ryu, L. Liu, S. Berciaud, Y. J. Yu, H. T. Liu, P. Kim, G. W. Flynn, L. E. Brus, *Nano Lett.* **2010**, *10*, 4944.